JACS
JOURNAL OF THE AMERICAN CHEMICAL SOCIETY

Communication

pubs.acs.org/JACS

On the Oxidation State of Manganese Ions in Li-Ion Battery Electrolyte Solutions

Anjan Banerjee,[†,§] Yuliya Shilina,[†,§] Baruch Ziv,[†] Joseph M. Ziegelbauer,[‡] Shalom Luski,[†] Doron Aurbach,[*,†] and Ion C. Halalay[⊥]

[†]Department of Chemistry, Bar-Ilan University, Ramat-Gan 5290002, Israel

[‡]Fuel Cell R&D, General Motors Global Propulsion Systems, Warren, Michigan 48092-2031, United States

[⊥]Chemical and Materials Systems Lab, General Motors Global R&D, Warren, Michigan 48092-2031, United States

Supporting Information

ABSTRACT: We demonstrate herein that Mn^{3+} and not Mn^{2+}, as commonly accepted, is the dominant dissolved manganese cation in $LiPF_6$-based electrolyte solutions of Li-ion batteries with lithium manganate spinel positive and graphite negative electrodes chemistry. The Mn^{3+} fractions in solution, derived from a combined analysis of electron paramagnetic resonance and inductively coupled plasma spectroscopy data, are ∼80% for either fully discharged (3.0 V hold) or fully charged (4.2 V hold) cells, and ∼60% for galvanostatically cycled cells. These findings agree with the average oxidation state of dissolved Mn ions determined from X-ray absorption near-edge spectroscopy data, as verified through a speciation diagram analysis. We also show that the fractions of Mn^{3+} in the aprotic nonaqueous electrolyte solution are constant over the duration of our experiments and that disproportionation of Mn^{3+} occurs at a very slow rate.

The prospects for dire consequences from global warming[1] spurred the development of battery-enhanced vehicles (XEVs) over the past 25 years. It is now clear that minimizing the pollution by automotive transportation must be based on Li-ion battery (LIB) technology,[2] also that the near- and medium-term XEV goals can only be achieved by a few materials: silicon−carbon composites and a subset of mixed transition metal (TM) oxides, respectively for negative and positive electrodes.[3−6] All TM oxides suffer from TM ions' dissolution, which is particularly acute at high temperatures and for materials with spinel structure, and results in reduced power performance as well as diminished charging/discharging capacity, hence a shortened battery life.[7−9]

Lithium manganate spinel ($Li_xMn_2O_4$, a.k.a. LMO)−graphite cells with $LiPF_6$ electrolyte solutions in organic carbonates are an ideal model system for studying the fundamental aspects of TM dissolution. The main mitigation measures proposed for the Mn dissolution issue to date are cation and anion substitutions in the LMO lattice,[7,8,10] surface coatings[11,12] and HF scavenging molecules.[13,14] None proved 100% effective. We hence proposed and showed that multifunctional (TM cation trapping, HF scavenging, and alkali metal ions dispensing) separators significantly improve the capacity retention in LMO−graphite cells during high-temperature cycling.[15−18] Because the cation trapping efficiency depends both on the nature of the chelating material and on the cation charge,[18] a knowledge of the TM ions' oxidation state in the electrolyte solution is essential for maximizing the LIB performance benefits conferred by these separators. Our work at this stage does not address any mechanisms for surface reactions or side reactions that cathodes may undergo during battery operation. We explore herein only the identity of relevant Mn ions that exist in the electrolyte solutions, in order to match them with the most effective trapping agents.

The disproportionation of Mn^{3+} ions in LMO ($2Mn^{3+} \leftrightarrows Mn^{2+} + Mn^{4+}$) with subsequent dissolution of Mn^{2+} ions into an aqueous acidic medium was first reported by Hunter in 1981.[19] Thackeray adopted this concept in 1994 and applied it to the LIB context.[10] However, such an extrapolation, from behavior in an aqueous solution to that in aprotic organic solvents lacks adequate backing by experimental data. Nevertheless, this uncontrolled transfer of concepts laid the foundation of the conceptual framework for the problem of Mn dissolution in LIBs for more than two decades. Several explanations for the Mn dissolution from LMO, all related to the disproportionation reaction were proposed over the years.[7,20−23] Note that Tarascon et al.[23] clearly stated a long time ago that the existence of Mn^{2+} in electrolyte solutions of LIBs is merely the most plausible hypothesis regarding the identity of the main dissolved Mn species, based on the behavior of Mn cations in aqueous solutions. (Ref 23 specifically states: "Even if the true composition of the soluble species is not known, it is reasonable to assume a Mn^{2+}-based species, because Mn^{2+} is the usual form of soluble manganese.") Still, a vast number of papers report various results pertaining to manganese ions in/on the negative or positive electrodes from LMO-containing cells, while merely assuming that Mn^{2+} is the sole dissolved species in the electrolyte solution. (See refs 24−29 for a sampling from the past four years.) In contrast, we know of only three previous studies aiming to determine the oxidation state of Mn ions in a Li-ion battery electrolyte solution.[30−32] Because a thorough investigation of Mn ions in a major LIB component (the electrolyte solution) was largely ignored, it is perhaps not surprising that the problem of Mn dissolution in Li-ion cells is still surrounded by controversy. Ref

Received: October 14, 2016
Published: January 25, 2017

DOI: 10.1021/jacs.6b10781
J. Am. Chem. Soc. 2017, 139, 1738−1741

30 concludes that that Mn^{2+} is the main species in the electrolyte solution. In contrast, our previous results[31,32] cast doubt on this conclusion. Although challenging the prevailing view regarding the oxidation state of Mn ions in LIB electrolyte solutions, refs 31 and 32 nevertheless present independent results obtained with similar but not identical electrode materials. Furthermore, the use of solid calibration standards for generating a calibration line for the average oxidation state <OS> vs relative Mn K-edge position in X-ray absorption near-edge spectroscopy (XANES) data raises some valid questions regarding the reliability of the conclusions from ref 31.

Herein we provide proof that Mn^{3+} and not Mn^{2+}, as commonly accepted, is the main soluble Mn ion species in the electrolyte solutions of LMO−graphite cells. We use a combined analysis of electronic paramagnetic resonance (EPR) plus inductively coupled plasma (ICP) spectroscopies[32] and XANES measurements to determine, respectively, the fraction of Mn^{3+} cations and their <OS> in electrolyte samples from identical LMO−graphite cells. In contrast to ref 31, we use an <OS> vs relative Mn K-edge position calibration line based on liquid oxidation state standards, thus removing some questions regarding the reliability of the XANES data analysis. We then demonstrate the consistency of the two sets of results through a speciation diagram analysis.

The electrolyte solution samples from the present study were a 1 M $LiPF_6$ solution in a 1:1 v/v binary mixture of ethylene carbonate (EC) and dimethyl carbonate (DMC), harvested from LMO−graphite cells after durations of 1 to 6 weeks, from one of the following electrochemical tests at 60 °C: (1) potential hold at 4.2 V (fully charged state); (2) potential hold at 3.0 V (fully discharged state); and (3) cycling at a current density corresponding to 5 h charging or discharging durations, between 3.0 and 4.2 V. EPR, ICP and XANES measurements were then performed on the Mn cations dissolved into each solution. Further details on cell assembly, electrochemical testing and cell disassembly, also EPR, ICP and XANES measurement procedures are provided in the Supporting Information.

Typical X-band EPR responses from Mn cations in the electrolyte solution are exemplified with data for the 4.2 V hold in Figure 1a. (See Figure S1 for the corresponding data for the 3.0 V hold and cycling experiments.) Figure 1a displays a sextet of hyperfine interaction lines, i.e., the signature for the EPR response from both Mn^{2+} and Mn^{4+} cations. The sextet results from the interaction of the ^{55}Mn nucleus (having a $3d^5$ electronic configuration with total spin $S = 5/2$) with the unpaired electrons.[33] Because the gyromagnetic factor of 2.0244 ± 0.0001 derived from the EPR data shown in Figures 1a and S1 corresponds to that for Mn^{2+} within a 0.005% uncertainty, one may conclude that the fraction of Mn^{4+} in the electrolyte solutions from all tested cells is zero. The next step in our analysis is to establish the correlation between the integrated EPR spectra (i.e., the doubly integrated EPR signal) and the total Mn amounts determined by ICP in a set of Mn^{2+} calibration samples with known Mn^{2+} amounts and then compare it against the same correlation for electrolyte solutions harvested from cells at the end of each test, as shown in Figure 1b. It is clear that the data points for the Mn ions in the electrolyte solution from all three tests fall well below the correlation line for the Mn^{2+} calibration solutions, indicative of the presence of Mn^{3+}, which is silent in EPR measurements. Constant Mn^{3+} fractions of ~80% exist in the electrolyte solution from either fully discharged (3.0 V hold) or fully charged (4.2 V hold) cells, and of ~60% in that from cycled cells, over the 6 weeks duration of each test, as shown in Figure 1c. Thus, although Mn^{3+} is the dominant Mn species in the solution, different operating protocols (cycling vs hold at low or high potentials) lead to different fractions of Mn^{3+} ions. This is likely due to the change in the relative abundances of Mn^{2+} and Mn^{3+} in the near-surface layers of LMO with state of charge and is currently still under investigation. Explaining these differences requires work that is beyond the scope of this communication.

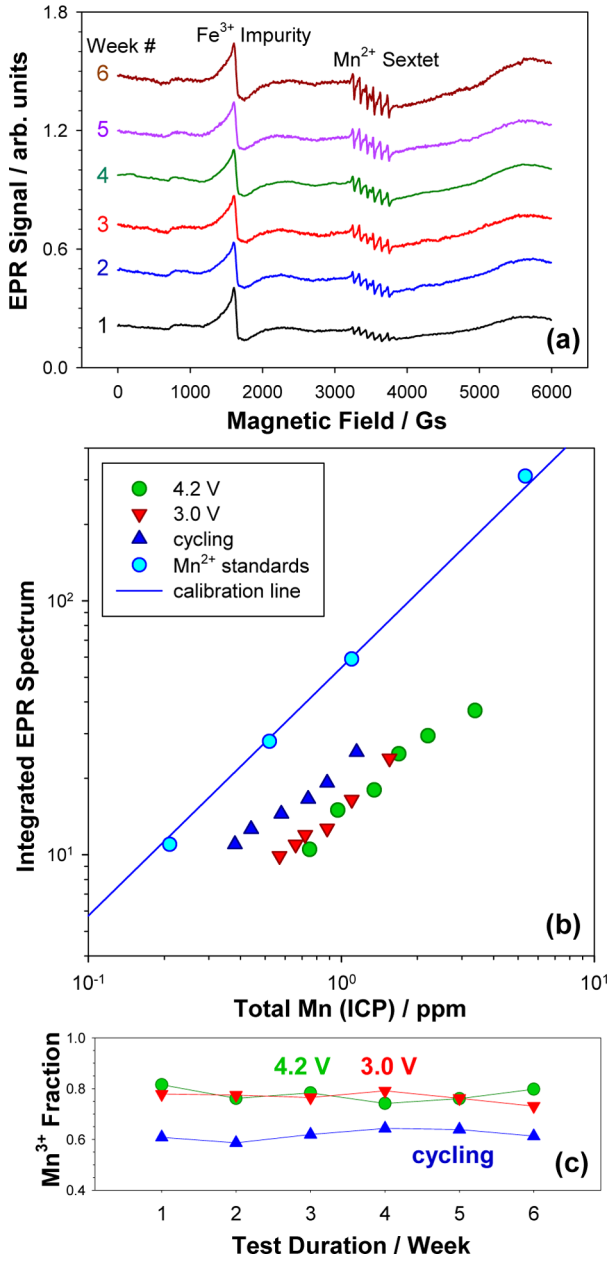

Figure 1. (a) EPR signals for electrolyte solutions from LMO−graphite cells subjected to 4.2 V holds for up to 6 weeks. (The spectra were shifted along the *y*-axis for legibility.) (b) Correlation between integrated EPR spectra and the total Mn determined by ICP. (c) Fraction of Mn^{3+} in the electrolyte solutions from cells subjected to cycling or potential holds at 60 °C.

We now address the issue of the Mn^{3+} disproportionation in the electrolyte solution. Hunter[24] showed that disproportionation of Mn^{3+} occurs in LMO when in contact with an acid

DOI: 10.1021/jacs.6b10781
J. Am. Chem. Soc. 2017, 139, 1738−1741

aqueous solution over a pH range of 1 to 5, followed by the dissolution of Mn^{2+} ions. The $LiPF_6$ electrolyte solution in a LIB is slightly acidic, due to trace amounts of HF and the Lewis acid PF_5. Mn^{3+} could therefore disproportionate, to form Mn^{2+} and Mn^{4+}. To investigate the disproportionation tendency of Mn^{3+} cations in aprotic organic solvents and electrolyte solutions, we carried out experiments with Mn(III) acetate salt solutions in EC-DMC (1:1) and in 1 M $LiPF_6$/EC-DMC (1:1). Mn^{3+} fractions were determined at room temperature (30 °C) by the EPR+ICP methodology in the as-prepared solutions, as well as after 1 and 3 months long stands. (For details, see Figures S2 and S3.) Neither Mn^{2+} nor Mn^{4+} were detected over a period 3 months in the Mn(III) acetate/EC:DMC solution. On the other hand, slow disproportionation was observed for Mn(III) acetate in 1 M $LiPF_6$/EC:DMC (1:1 v/v), with 97%, 88% and 83% of the initial Mn^{3+} present, respectively, 15 min subsequent to preparation, and after 1 month and 3 months long stands. Thus, disproportionation of Mn^{3+} does indeed occur in the $LiPF_6$ solution, albeit at a rather small rate. In contrast, the Mn^{3+} fractions in the electrolyte solutions from the three tests were practically constant over the 6 weeks duration of the electrochemical experiments (Figure 1c), with no evidence for Mn^{4+} present. Because Mn^{4+} is a strong oxidizer, it is likely to oxidize solvent molecules very rapidly and thus be reduced to Mn^{3+} before accumulating in amounts large enough to be detectable by EPR. Nonetheless, the amount of Mn^{3+} would steadily decrease over time if disproportionation were to occur with any significant rate. It is therefore necessary to inquire into mechanisms at play in LMO−graphite cells that counteract disproportionation, to keep the Mn^{3+} fraction constant. Possible stabilization mechanisms for the Mn^{3+} concentration are being investigated with computational modeling at present. Further clues regarding the source for the large fraction of Mn^{3+} in our experiments may come from the work of Tang et al.,[28] who report the formation of a Mn_3O_4 spinel surface phase in LMO, a result confirmed by Amos and co-workers.[29]

Figure 2a displays XANES spectra for electrolyte filled separators from cells subjected to the three electrochemical tests, together with spectra for three oxidation state calibration standards (Mn^0 metal, Mn^{2+} and Mn^{3+} fluoride solutions in EC:DMC 1:1 v/v). The oxidation state of Mn ions in the electrolyte-filled separators exceeds +2 and is smaller than +3, as can be readily seen from the relative positions of the rising part of the main peak in the spectra. The positon of the Mn K-edge in all three electrolyte samples (as determined from the maxima in the first derivative $d\mu/dE$) is shown in Figure 2b. The positions of the maxima in $d\mu/dE$ for the three calibration standards were used for generating the <OS> vs $E_{0,rel}$ calibration line displayed in Figure 2c. We find an average oxidation state of +2.6 ± 0.2 for Mn ions in the electrolyte solution, irrespective of test type. (More details regarding the XANES methodology can be found in the Supporting Information.)

A speciation diagram analysis (Figure 3) was conducted for the Mn ions in the electrolyte solutions, based on the eqs $2x_2 + 3x_3 + 4x_4 = <OS>$ and $x_2 + x_3 + x_4 = 1$ (where x_2, x_3 and x_4 are, respectively, the atomic fractions of Mn^{2+}, Mn^{3+} and Mn^{4+}). The speciation diagram indicates that the values derived for the Mn^{3+} fraction through the EPR+ICP analysis and the <OS> derived from the XANES data are compatible with the following cation compositions: $(x_2, x_3, x_4) \in \{(0.2, 0.8, 0), (0.3, 0.6, 0.1), (0.4, 0.6, 0)\}$. However, because the values for the gyromagnetic factor derived from the EPR measurements correspond exactly to that of Mn^{2+} ions, one has $x_4 = 0$, hence (0.3, 0.6, 0.1) must be rejected as a possible composition.

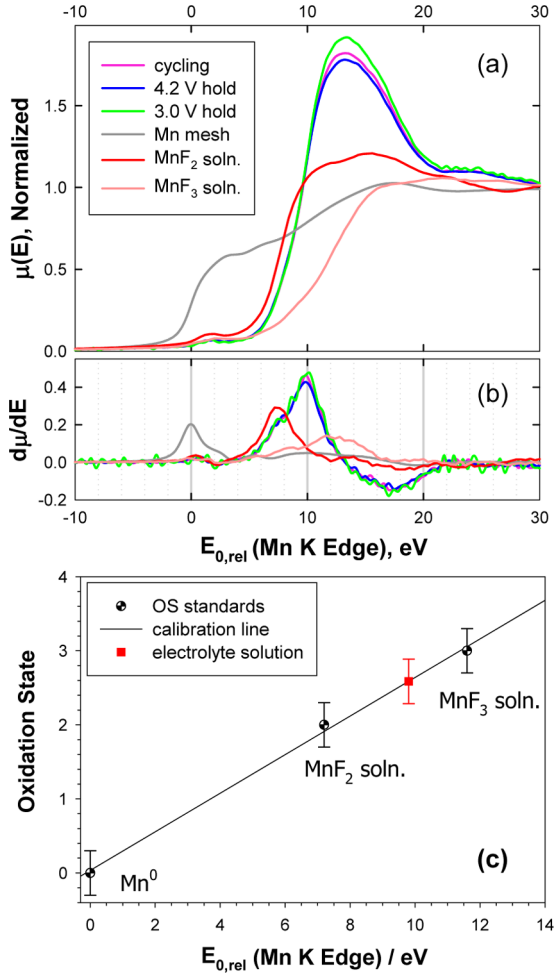

Figure 2. (a) XANES spectra for electrolyte-filled separators from three tested cells and three oxidation state standards (Mn metal mesh; Mn^{2+} and Mn^{3+} fluoride solutions in EC:DMC 1:1). (b) First derivative of the XANES spectra with respect to energy. (c) Determining the average oxidation state of the Mn ions in electrolyte solutions from cells subjected to electrochemical tests. The red square marks three overlapping data points from three distinct measurements. Calibration line equation: $<OS> = 0.03412 + 0.2605\ E_{0,rel}$, $R^2 = 0.997$.

In conclusion, the combined ICP+EPR and XANES methodologies show unambiguously that Mn^{3+} is the major species in the $LiPF_6$ electrolyte solution and that its amounts depends on the electrochemical test conditions. The observed differences may result from the combined effect of the relative solubility of Mn^{3+} and Mn^{4+} ions in the electrolyte solution, and from changes in their relative abundance in LMO with state of charge. We hypothesize that the greater solvation stability of Mn^{3+} over Mn^{2+} overcomes the slow disproportionation tendency of the former, resulting in Mn^{3+} being the dominant Mn ion in solution. Our results contradict the conventional description, which depicts Mn^{2+} as sole electrolyte soluble species. Furthermore, our findings call into question Mn^{3+} disproportionation as a major mechanism for the manganese cations' dissolution from LMO, perhaps also from other Mn-rich positive electrode materials for LIBs with spinel phases.

DOI: 10.1021/jacs.6b10781
J. Am. Chem. Soc. 2017, 139, 1738−1741

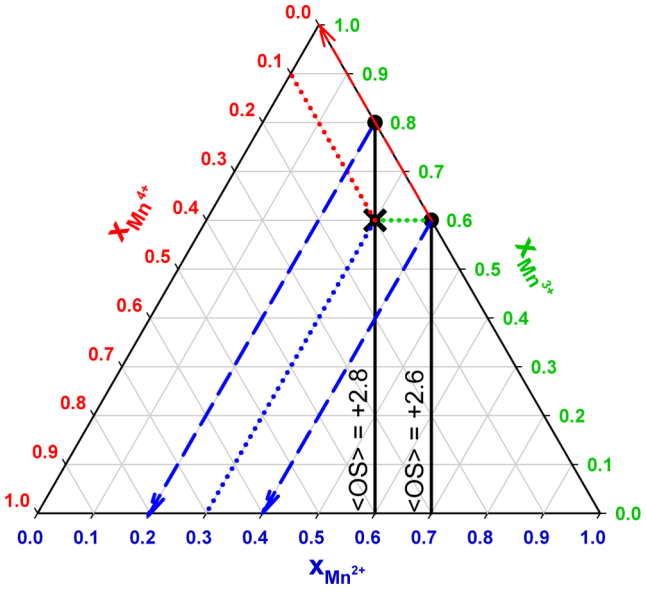

Figure 3. Ternary speciation diagram for Mn cations in the electrolyte solution, displaying the <OS> = +2.6 and <OS> = +2.8 lines. The two dots mark the compositions that are consistent with all the EPR+ICP and XANES results. The colored interrupted and dotted lines ending with an arrow are guides for reading the diagram. The "×" symbol and dotted lines mark the rejected speciation, because the EPR data show that $x_4 = 0$.

■ ASSOCIATED CONTENT

Supporting Information

The Supporting Information is available free of charge on the ACS Publications website at DOI: 10.1021/jacs.6b10781.

Electrodes preparation, cell assembly, electrochemical test procedures; details of EPR, ICP and XANES analyses (PDF)

■ AUTHOR INFORMATION

Corresponding Author

*aurbach@biu.ac.il

ORCID

Anjan Banerjee: 0000-0002-5658-4610

Doron Aurbach: 0000-0002-1151-546X

Author Contributions

§These authors contributed equally.

Notes

The authors declare no competing financial interest.

■ ACKNOWLEDGMENTS

The Israel Science Foundation provided partial support for this work in the framework of the INREP project. The authors thank Dr. Raghunathan K. for critically reading the paper and useful suggestions. Sungsik Lee and Benjamin Reinhart assisted in the setup and operation of the APS beamline at sector 12-BM. This work used resources of the Advanced Photon Source, a U.S. Department of Energy (DOE) Office of Science User Facility operated for the DOE Office of Science by Argonne National Laboratory under Contract No. DE-AC02-06CH11357.

■ REFERENCES

(1) Levasseur, A.; Cavalett, O.; Fuglestvedt, J. S.; Gasser, T.; Johansson, D. J. A.; Jørgensen, S. V.; Raugei, M.; Reisinger, A.; Schivley, G.; Strømman, A.; Tanaka, K.; Cherubini, F. *Ecol. Indic.* **2016**, *71*, 163.

(2) Yong, J. Y.; Ramachandaramurthy, V. K.; Tan, K. M.; Mithulananthan, N. *Renewable Sustainable Energy Rev.* **2015**, *49*, 365.

(3) Manthiram, A.; Knight, J. K.; Myung, S.-T.; Oh, S.-M.; Sun, Y.-K. *Adv. Energy Mater.* **2016**, *6*, No. 1501010.

(4) Yoon, C. S.; Choi, M. H.; Lim, B.-B.; Lee, E.-J.; Sun, Y.-K. *J. Electrochem. Soc.* **2015**, *162*, A2483.

(5) Luo, F.; Liu, B.; Zheng, J.; Chu, G.; Zhong, K.; Li, H.; Huang, X.; Chen, L. *J. Electrochem. Soc.* **2015**, *162*, A2509.

(6) USABC EV and PHEV Battery Goals, at http://www.uscar.org/guest/article_view.php?articles_id=85.

(7) Amatucci, G.; Du Pasquier, A.; Blyr, A.; Zheng, T.; Tarascon, J. M. *Electrochim. Acta* **1999**, *45*, 255.

(8) Choi, W.; Manthiram, A. J. *J. Electrochem. Soc.* **2006**, *153*, A1760.

(9) Tsujikawa, T.; Yabuta, K.; Matsushita, T.; Arakawa, M.; Hayashi, K. *J. Electrochem. Soc.* **2011**, *158*, A322.

(10) Gummow, R. J.; De Kock, A.; Thackeray, M. M. *Solid State Ionics* **1994**, *69*, 59−67.

(11) Li, C.; Zhang, H. P.; Fu, L. J.; Liu, H.; Wu, Y. P.; Rahm, E.; Holze, R.; Wu, H. Q. *Electrochim. Acta* **2006**, *51*, 3872.

(12) Jung, Y. S.; Cavanagh, A. S.; Riley, L. A.; Kang, S. H.; Dillon, A. C.; Groner, M. D.; George, S. M.; Lee, S. H. *Adv. Mater.* **2010**, *22*, 2172.

(13) Xu, K. *Chem. Rev.* **2004**, *104*, 4303.

(14) Xu, K. *Chem. Rev.* **2014**, *114*, 11503.

(15) Banerjee, A.; Ziv, B.; Shilina, Y.; Luski, S.; Aurbach, D.; Halalay, I. C. *J. Electrochem. Soc.* **2016**, *163*, A1083.

(16) Banerjee, A.; Ziv, B.; Shilina, Y.; Luski, S.; Halalay, I. C.; Aurbach, D. *Adv. Energy Mater.* **2016**, No. 1601556.

(17) Banerjee, A.; Ziv, B.; Luski, S.; Aurbach, D.; Halalay, I. C. *J. Power Sources* **2017**, *341*, 457.

(18) Banerjee, A.; Ziv, B.; Ziegelbauer, J. M.; Luski, S.; Aurbach, D.; Halalay, I. C.; Shilina, Y. *J. Electrochem. Soc.* **2017**, *164*, A6315.

(19) Hunter, J. C. *J. Solid State Chem.* **1981**, *39*, 142.

(20) Jang, D. H.; Oh, S. M. *J. Electrochem. Soc.* **1997**, *144*, 3342.

(21) Xia, Y.; Zhou, Y.; Yoshio, M. *J. Electrochem. Soc.* **1997**, *144*, 2593.

(22) Choa, J.; Thackeray, M. M. *J. Electrochem. Soc.* **1999**, *146*, 3577.

(23) Blyr, A.; Sigala, C.; Amatuci, G.; Guyormard, D.; Chabre, Y.; Tarascon, J.-M. *J. Electrochem. Soc.* **1998**, *145*, 194.

(24) Ochida, M.; Doi, T.; Domi, Y.; Tsubouchi, S.; Nakagawa, H.; Yamanaka, T.; Abe, T.; Ogumi, Z. *J. Electrochem. Soc.* **2013**, *160*, A410.

(25) Zhan, C.; Lu, J.; Kropf, A. J.; Wu, T.; Jansen, A. N.; Sun, Y.-K.; Qiu, X.; Amine, K. *Nat. Commun.* **2013**, *4*, No. 2437.

(26) Gowda, S. R.; Gallagher, K. G.; Croy, J. R.; Bettge, M.; Thackeray, M. M.; Balasubramanian, M. *Phys. Chem. Chem. Phys.* **2014**, *16*, 6898.

(27) Shkrob, I. A.; Kropf, A. J.; Marin, T. W.; Li, Y.; Poluektov, O. G.; Niklas, J.; Abraham, D. P. *J. Phys. Chem. C* **2014**, *118*, 24335.

(28) Tang, D.; Sun, Y.; Yang, Z.; Ben, L.; Gu, L.; Huang, X. *Chem. Mater.* **2014**, *26*, 3535.

(29) Amos, C. A.; Roldan, M. A.; Varela, M.; Goodenough, J. B.; Ferreira, P. J. *Nano Lett.* **2016**, *16*, 2899.

(30) Terada, Y.; Nishiwaki, Y.; Nakai, I.; Nishikawa, F. *J. Power Sources* **2001**, *97*−*98*, 420.

(31) Li, Z.; Pauric, A. D.; Goward, G. R.; Fuller, T. J.; Ziegelbauer, J. M.; Balogh, M. P.; Halalay, I. C. *J. Power Sources* **2014**, *272*, 1134.

(32) Shilina, Y.; Ziv, B.; Meir, A.; Banerjee, A.; Ruthstein, S.; Luski, S.; Aurbach, D.; Halalay, I. C. *Anal. Chem.* **2016**, *88*, 4440.

(33) Weil, J. A.; Bolton, J. R. *Electron Paramagnetic Resonance: Elementary Theory and Practical Applications*, 2nd ed.; John Wiley & Sons: Hoboken, NJ, 2007.

DOI: 10.1021/jacs.6b10781
J. Am. Chem. Soc. 2017, 139, 1738−1741